Effect of growth parameters on the morphology and optical properties of ZnO nanocolumn arrays

WENYANG MA[1], LINHUA XU[1,2,*], AOXIN ZANG[1], ZHEN TIAN[1]
[1]*School of Physics and Optoelectronic Engineering, Nanjing University of Information Science & Technology, Nanjing 210044, China*
[2]*Laboratory for Optoelectronic Functional Materials and Devices，Nanjing University of Information Science & Technology, Nanjing 210044, China*

As a functional material, ZnO nanocolumns will be widely used in optoelectronic and microelectronic devices, but the research on ZnO nanocolumns produced by hydrothermal method has been rarely reported. In this study, we used hydrothermal method to grow ZnO nanocolumn arrays under different parameters (seed-layer thickness, growth time, zinc source), and compared their structure, morphology and optical properties. These ZnO nanocolumns exhibit good homogeneity and crystalline quality. The increase of seed-layer thickness and growth time is beneficial to obtain nanocolumn arrays with high transmittance and good alignment along the c-axis. The photoluminescence spectra show that the samples have strong yellow-green and red emissions, which makes them potentially useful in display devices.

(Received February 11, 2023; accepted February 12, 2024)

Keywords: Zinc nanocolumns, Hydrothermal method, Absorption spectra, Optical bandgap, Photoluminescence

1. Introduction

The new-generation of microelectronics and optoelectronic devices often need to meet the requirements of light weight, high strength, and low energy consumption. Therefore, nanostructured materials will play a very important role in the new generation of microelectronics and optoelectronic devices. There are many kinds of nanomaterials, including nanowires, nanosheets, nanofibers, nanorods, nanotubes, nanocolumns, etc. [1-5]. Among them, metal-oxide nanocolumns have attracted much attention from researchers because of their excellent physical properties [6-10]. For example, Li et al. [11] prepared $La_{0.67}Sr_{0.33}MnO_3$ films with epitaxial nanocolumn arrays by self-assembly method, which exhibit adjustable magnetic properties. Singh et al. [12] synthesized In_2O_3-SiO_x nanocolumn arrays using GLAD, which have good humidity sensing performance. Mamat et al. [13] obtained ZnO nanocolumnar arrays by magnetron sputtering. They found that by changing the oxygen flow rate, the structural characteristics such as the length of those nanocolumns can be adjusted to change their optical properties and ultraviolet sensing performance. Meng et al. [14] synthesized CeO_2 nanocolumns by hydrothermal method, which showed good room temperature ferromagnetism. Pietrzyk et al. [15] prepared ZnMgO nanocolumns through MBE technology, which showed good UV emission performance.

Among many nanocolumns materials, ZnO nanocolumns have attracted wide attention due to their excellent optical and electronic properties [15-17]. By consulting the literatures, it is known that the reported ZnO nanocolumns are mostly prepared by magnetron sputtering [10, 13], MBE [15], vapor transport [16] and other methods. The cost of preparing ZnO nanocolumns using the above methods is high. Due to the simple equipment and low cost, hydrothermal method has been widely used to prepare nanostructured materials. For example, Meng et al. [14] synthesized CeO_2 nanocolumns by hydrothermal method. However, ZnO nanocolumns grown by hydrothermal method are rarely reported. In this study, ZnO nanocolumns were grown by hydrothermal method, and the effect of growth parameters on the structure and optical properties of ZnO nanocolumns were revealed. The results reported in this paper are helpful for the development of ZnO-based micro-nano devices in the future.

2. Experimental

2.1. Growth of ZnO nanocolumns by hydrothermal method

In order to understand the effect of zinc source on ZnO nanocolumns, zinc nitrate and zinc acetate were used for comparison. In the growth solution, the concentration of Zn ion was 0.05 mol/L. Hexamethylenemethine with the same concentration as zinc ion was added to the growth solution as an alkali source. The mixture produced above and a glass slide with a pre-deposited ZnO seed layer were put into a hydrothermal autoclave and kept at 90 ℃ for different times to reveal the effect of growth time. A total of four different samples were prepared. For clarity, the four sample names and their growth conditions

are listed in Table 1. Once the set growth time was reached, the samples were removed from the hydrothermal autoclave, washed with ethanol and demonized water for three times, and then dried by an infrared lamp. The samples were not post-annealed.

2.2. Apparatus or methods to characterize sample properties

The structural properties of the nanocolumn arrays were analyzed by XRD using Bruker D8 diffractometer. The morphological features were analyzed by FE-SEM (S-4800). The chemical composition was determined by XPS. The transmittance and absorption spectra were recorded by UV-Vis spectrophotometer (TU-1901). The photoluminescence behavior of the samples was studied by a spectral detector (LabRAM HR800) using He-Cd laser as light source.

3. Results and discussion

3.1. The morphology, phase and composition of the samples

Fig. 1 displays the morphology images of the samples produced by hydrothermal method. It can be noticed that dense nanocolumn arrays have been grown on the ZnO seed-layer. From the top-view images, it can be clearly seen that these nanocolumns are hexagonal in plane.

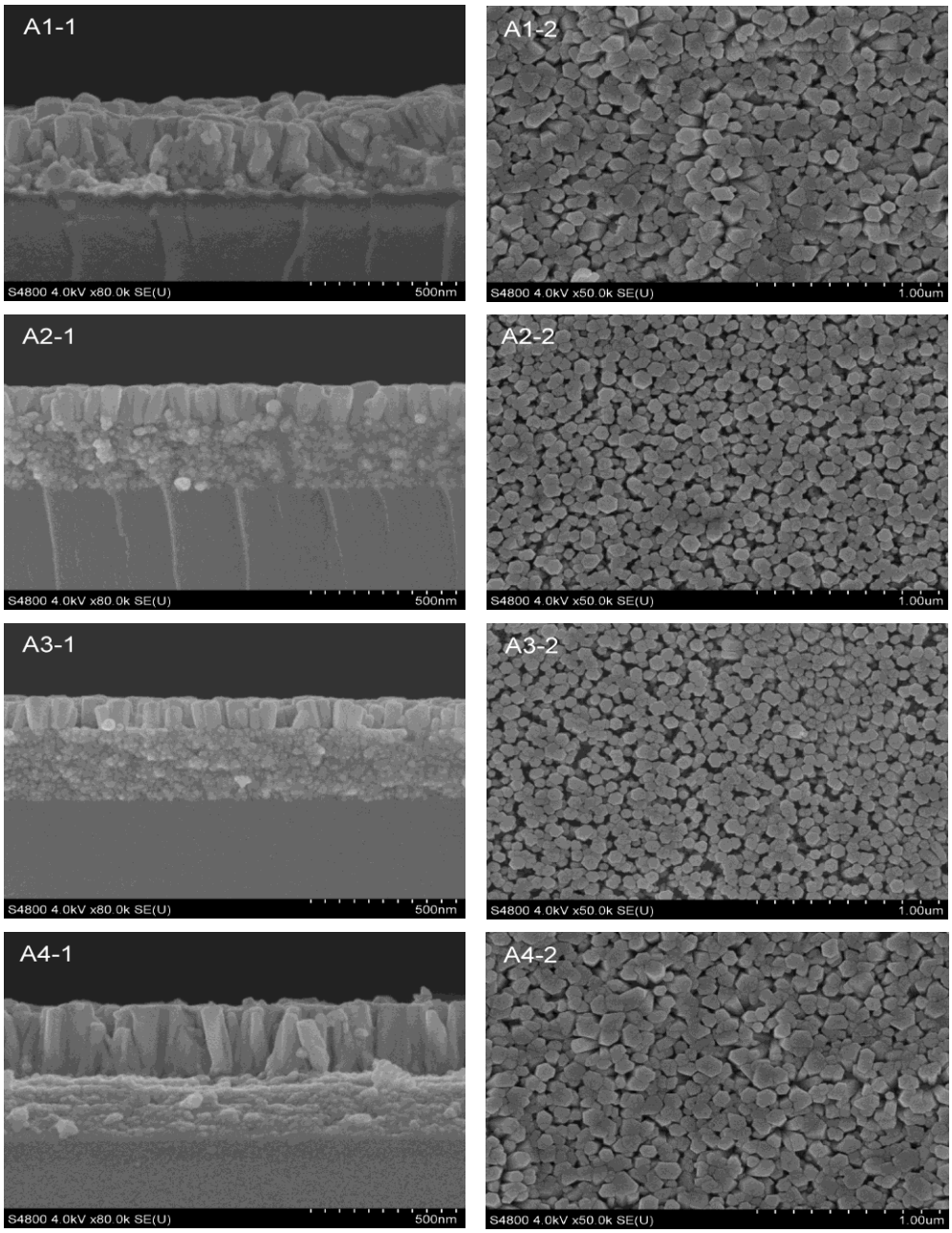

Fig. 1. Morphology images of ZnO nanocolumns grown by hydrothermal method

Compared with sample A1, the alignment of nanocolumns for other samples is more orderly, and almost every nanocolumn is perpendicular to the substrate surface, which indicates that the thicker seed-layer is more favorable to grow regularly aligned nanocolumns. A2 and A3 are the samples with the same thickness seed-layer and the same growth time. There is basically no difference in appearance for A2 and A3, except that the diameter of the nanocolumns grown with the solution containing zinc acetate is slightly thicker than that grown with the solution containing zinc nitrate. Such results have also been reported by other researchers [18]. Compared with other nanocolumns, the ones in sample A4 are longer, which is due to the longer growth time.

Fig. 2 shows the XRD patterns of ZnO nanocolumns. These patterns reveal that all the ZnO nanocolumns exhibit a high growth-orientation along the (002) plane regardless of the growth parameters, which means they are highly c-axis oriented. With the extension of growth time, the (002) diffraction peak of ZnO nanocolumns is gradually increased, which is due to the increase of the length of the nanocolumns and the higher alignment along the c-axis direction. This is consistent with the SEM observation results. Fig. 3 shows the XPS spectra of sample A2. The carbon signal in the energy spectrum should come from the carbon-containing substances in the air adsorbed on the sample surface. The high-resolution O 1s energy spectrum is obviously not geometrically symmetrical, indicating that the oxygen on the surface of ZnO nanocolumns is in different chemical states. After Gaussian fitting, it is found that the O 1s line is composed of several sub-peaks. The sub-peak at 530 eV is derived from the lattice oxygen bonded to Zn^{2+} [19]; the sub-peak at 531.3 eV is usually ascribed to oxygen vacancies (V_O) [20]; and the sub-peak at high-energy position (532.2 eV) is believed to be derived from oxygen-containing substances such as hydroxyl groups adsorbed on the surface of ZnO [19, 20]. The existence of lots of oxygen vacancies on ZnO surface has different significance for different applications. For the ZnO-based UV light-emitting devices, lots of surface oxygen vacancies are harmful. However, for ZnO-based photocatalysts or gas sensors, a great number of surface oxygen vacancies may be advantageous [21].

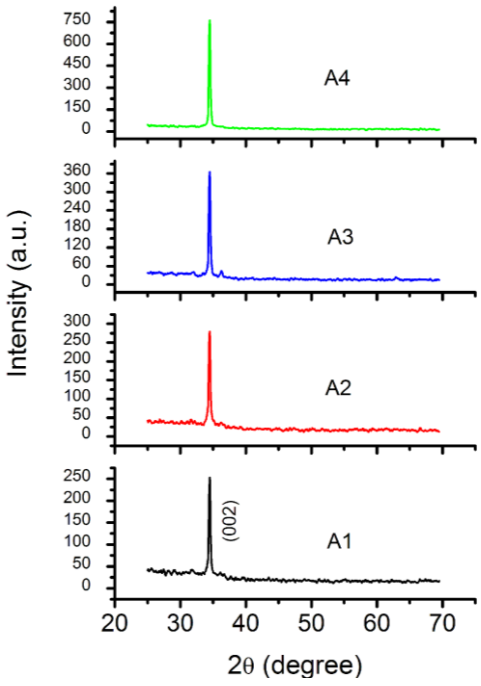

Fig.2 XRD patterns of the samples (color online)

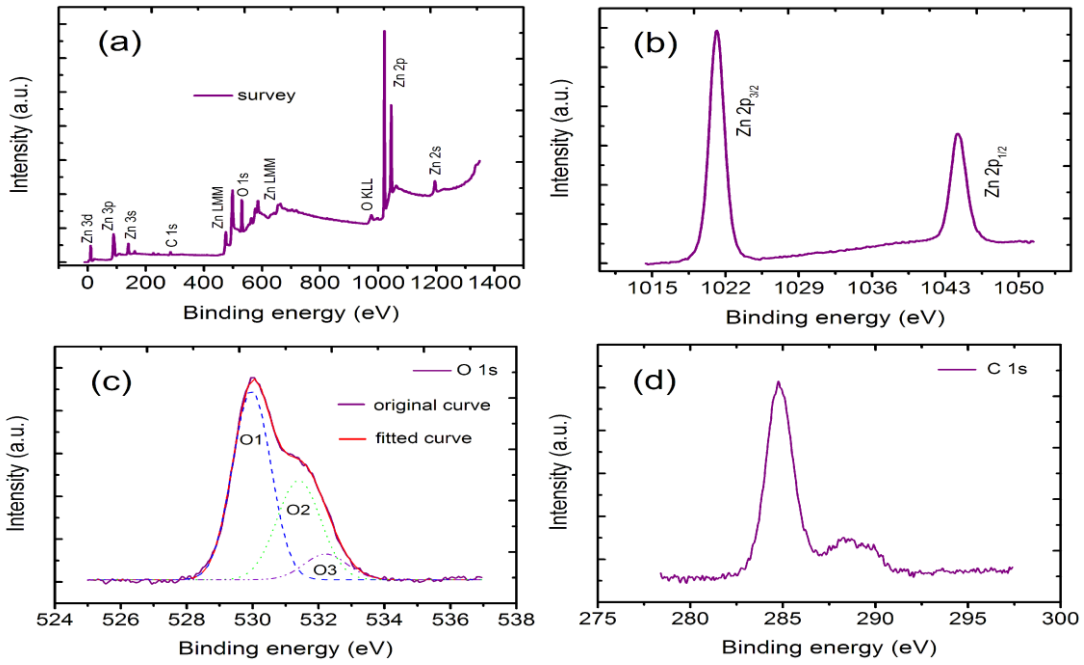

Fig. 3. Typical XPS spectra of A2 (color online)

3.2. The optical properties of the samples

Fig. 4 displays the transmittance spectra of the samples. A1 sample shows the lowest transmittance, while the transmittance of other samples has been greatly improved. This is due to the more orderly arrangement of ZnO nanocolumns in A2, A3 and A4.

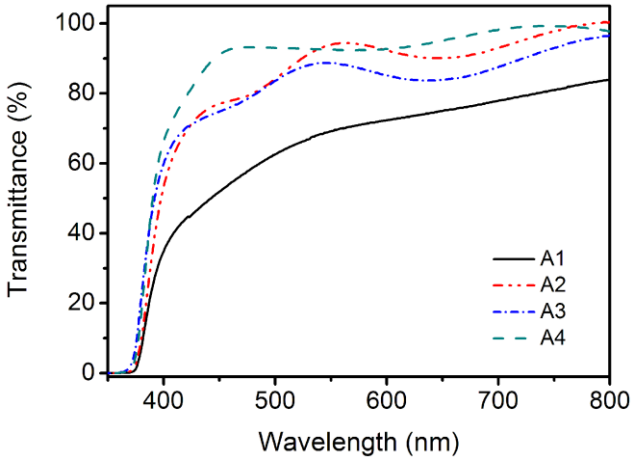

Fig. 4. Transmittance spectra of the samples (color online)

Fig. 5 gives absorption spectra for the samples and the optical bandgaps derived from the absorption spectra. All the samples exhibit low absorption in the range of 400-800 nm as shown in Fig. 5 (a). It is concluded that the higher the alignment of nanocolumns is, the lower the absorption of visible-light is. This is because if the alignment of the nanocolumns is higher, the less light will be scattered between the nanocolumns and correspondingly less light will be absorbed. The optical bandgaps of the samples are about 3.20 eV, with little difference. They are close to the bandgaps of ZnO nanostructures grown by hydrothermal method reported by others. For example, the bandgap of ZnO nanorods prepared by Zirak et al. is 3.28 eV [22]; the bandgap of ZnO nanopowders synthesized by Robkhob et al. is 3.25 eV [23]. The difference in bandgaps comes from different deposition conditions, annealing treatments, and doping impurities.

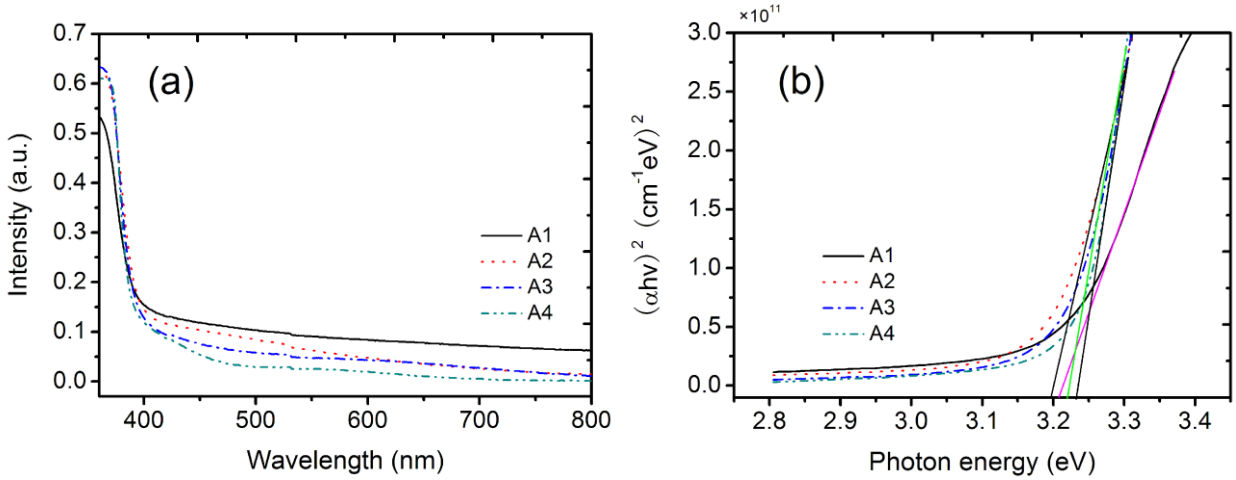

Fig. 5. (a) Absorption spectra and (b) bandgaps of the samples (color online)

The light emission of ZnO nanomaterials has received extensive attention of lots of researchers. Due to the abundance of ZnO raw materials, the ease of preparation of nanomaterials, and the diversity of emission wavelengths, ZnO has great potential application in solid-state white light-emitting devices and display devices. Fig. 6 (a) shows the photoluminescence spectra of the samples. The samples display a weak UV emission with a strong visible emission; it is similar to the luminescence behavior of many ZnO nanomaterials prepared by hydrothermal method [23-25]. In order to determine the visible emission centers, we select the spectral line of A2 for Gaussian fitting, as shown in Fig. 6 (b). It shows three visible emission centers with wavelengths of 526, 569 and 626 nm respectively. This is very similar to the luminescence behavior of pure ZnO and Ni doped ZnO nanoparticles prepared by hydrothermal method reported by Robkhob et al. [23]. ZnO with this characteristic luminescence behavior may have a potential application in displays [26]. The green emission of ZnO has been widely explored. Although there is no consensus on its emission mechanism, most researchers suggest that it is related to the single ionized V_O defect [20, 27]. Moreover, the above XPS spectrum of A2 confirms the existence of surface V_O. Therefore, we believe that the green emission at 526 nm originates from the electron transition related to the energy level of single ionized V_O. For the yellow-green emission at 569 nm, some researchers suggest that it is bound up with the double ionized V_O [28]. For the red emission with a wavelength of 626 nm, it may be related to the hydroxyl or oxygen adsorbed on the ZnO surface [26]. As the growth time increases, the UV emission is enhanced, while the visible emission is weakened significantly. This

means that with the increase of growth time, the lattice defects on the surface of ZnO nanocolumns are reduced and the crystallinity is improved.

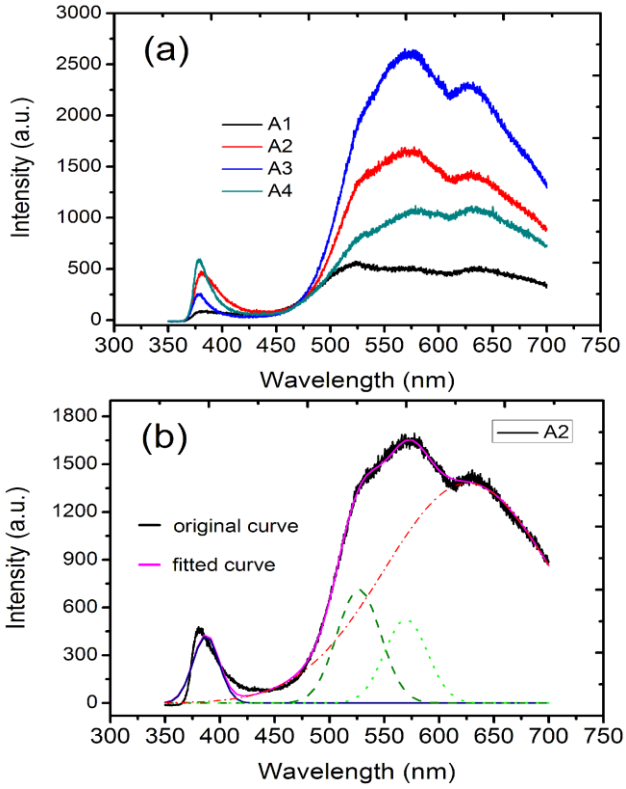

Fig. 6. (a) Photoluminescence spectra and (b) Gaussian fitting of the spectral line of A2 (color online)

Table 1. ZnO nanocolumns grown by hydrothermal method and their growth conditions

Sample name	Zinc source	Growth time	Seed layer thickness
A1	Zinc acetate	1.0 h	120 nm
A2	Zinc acetate	1.0 h	250 nm
A3	Zinc nitrate	1.0 h	250 nm
A4	Zinc acetate	1.5 h	250 nm

4. Conclusions

In this study, ZnO nanocolumns were fabricated using hydrothermal method. The experimental results show that the thicker seed-layer is more conducive to obtain ZnO nanocolumns with high transmittance and better alignment along the c-axis. The extension of the growth time increases the length of the nanocolumns, reduces the defects on the surface of the nanocolumns, and improves the crystal quality. Using zinc nitrate or zinc acetate as the zinc source has little effect on the morphology, optical transmittance and bandgap of ZnO nanocolumns. The optical bandgap of these ZnO nanocolumns is around 3.22 eV. The nanocolumns show strong yellow-green and red emission.

Acknowledgements

This work is supported by the excellent graduation thesis support-project in 2024 from Nanjing University of Information Science and Technology and the special funds for connotation construction and development of higher education in Jiangsu Province of China (Grant no. XJDCZX202110300062).

References

[1] W. Zhang, R. Chen, X. Zhu, D. Ye, Y. Yang, Y. Yu, Y. Liu, Q. Liao, Journal of Power Sources **555**, 232377 (2023).
[2] V. K. Singh, C. M. Patel, Inorganic Chemistry Communications **149**, 110440 (2023).
[3] M. Davoodi, K. Abbassian, J. Tizfahm, M. H. Yousefi, J. Optoelectron. Adv. M. **22**(3-4), 95 (2020).
[4] Susana Mihaiu, Oana Cătălina Mocioiu, Alexandra Toader, Irina Atkinson, Jeanina Pandele Cuşu, Cornel Munteanu, Maria Zaharescu, Rev. Roum. Chim. **61**, 485 (2016).
[5] R. C. Yang, Z. D. Fan, X. P. Geng, G. L. Wang, F. Wang, Optoelectron. Adv. Mat. **16**(1-2), 74 (2022).
[6] M. Sepúlveda, J. G. Castaño, F. Echeverría, Materials Chemistry and Physics **216**, 51 (2018).
[7] S. Najwa, A. Shuhaimi, N. Ameera, K. M. Hakim, M. Sobri, M. Mazwan, M. H. Mamat, Y. Yusnizam, V. Ganesh, M. Rusop, Superlattices and Microstructures **72**, 140 (2014).
[8] A. Nouri, A. Beniaiche, B. M. Soucase, H. Guessas, A. Azizi, Optik **139**, 104 (2017).
[9] T. Horide, A. Ichinose, F. Tokura, K. Matsumoto, Thin Solid Films **733**, 138802 (2021).
[10] H. Zhang, C. Lou, X. Huang, H. Yang, Optical Materials **122**, 111716 (2021).
[11] J. Li, J. Wu, L. Shen, J. Yang, L. Lu, C. Cao, C. Jiang, X. Lu, L. Zhang, H. Yu, M. Liu, Materials Today Physics **13**, 100218 (2020).
[12] N. K. Singh, B. Choudhuri, A. Monda, J. C. Dhar, T. Goswami, S. Saha, C. Ngangbam, Electron. Mater. Lett. **10**, 975 (2014).
[13] M. H. Mamat, M. F. Malek, N. N. Hafizah, M. N. Asiah, A. B. Suriani, A. Mohamed, N. Nafarizal, M. K. Ahmad, M. Rusop, Ceramics International **42**, 4107 (2016).
[14] F. Meng, C. Zhang, Q. Bo, Q. Zhang, Materials Letters **99**, 5 (2013).
[15] M. A. Pietrzyk, M. Stachowicz, P. Dluzewski, A. Wierzbicka, A. Kozanecki, Journal of Alloys and Compounds **737**, 748 (2018).
[16] T. Trad, P. Blount, Z. Romero, D. Thompson, MRS Advances **5**, 1687 (2020).
[17] A. Baez-Rodríguez, L. Zamora-Peredo, M. G. Soriano-Rosales, J. Hernandez-Torres, L. García-Gonzalez, R. M. Calderon-Olvera, M. García-Hipolito, J. Guzman-Mendoza, C. Falcony, Journal of Luminescence **218**,

116830 (2020).
[18] A. C. Catto, M. M. Ferrer, O. F. Lopes, V. R. Mastelaro, J. Andrés, L. F. da Silva, E. Longo, W. Avansi Jr., Applied Surface Science **529**, 147057 (2020).
[19] C. Yu, Y. Yu, T. Xu, X. Wang, M. Ahmad, H. Sun, Materials Letters **190**, 185 (2017).
[20] U. Ilyas, P. Lee, T. L. Tan, R. Chen, A. W. Anwar, S. Zhang, H. D. Sun, R. S. Rawat, Applied Surface Science **387**, 461 (2016).
[21] F. Yu, Z. Liu, Y. Li, D. Nan, B. Wang, L. He, J. Zhang, X. Tang, H. Duan, Y. Liu, Applied Physics A **126**, 931 (2020).
[22] M. Zirak, O. Akhavan, O. Moradlou, Y. T. Nien, A. Z. Moshfegh, Journal of Alloys and Compounds **590**, 507 (2014).
[23] P. Robkhob, I. M. Tang, S. Thongmee, Materials Science and Engineering B **260**, 114644 (2020).
[24] Y. Lei, F. Qu, X. Wu, Nano-Micro Letters **4**(1), 45 (2012).
[25] J. Ungula, H. C. Swart, Journal of Alloys and Compounds **821**, 153459 (2020).
[26] S. Alamdari, M. J. Tafreshi, M. S. Ghamsari, Applied Physics A **125**, 165 (2019).
[27] P. K. Giri, S. Dhara, R. Chakraborty, Materials Chemistry and Physics **122**, 18 (2010).
[28] M. A. Khan, M. K. Singha, K. K. Nanda, S. B. Krupanidhi, Applied Surface Science **505**, 144365 (2020).

*Corresponding author: congyu3256@sina.com